

Article

Day-Ahead Forecasting of the Theoretical and Actual Wind Power Generation in Energy-Constrained Island Systems

Konstantinos Moustris ^{1,*}  and Dimitrios Zafirakis ² 

¹ Air Pollution Lab., Department of Mechanical Engineering, University of West Attica, 250 Thivon & P. Ralli Street, 12241 Athens, Greece

² Soft Energy Applications & Environmental Protection Lab., Mechanical Engineering Department, University of West Attica, 250 Thivon & P. Ralli Street, 12241 Athens, Greece; dzaf@uniwa.gr

* Correspondence: kmoustris@uniwa.gr; Tel.: +30-2105381234

Abstract: Grid operators of islands with limited system tolerance are often challenged by the need to curtail wind energy in order to maintain system stability and security of supply. At the same time, and in the absence of storage facilities and/or other means of flexibility such as demand-side management, wind park owners face the problem of rejected wind energy production that varies considerably within the year. In the prospect of a more dynamic market operation in island grids, estimation of the anticipated wind energy curtailments may allow the evaluation of different options for wind park owners, such as short-term leasing of energy storage and/or direct, bilateral power purchase agreements with flexible demand entities. To enable such options, effective wind energy forecasting is necessary not only in terms of theoretical production, but also in terms of actual production being absorbed by the system. In this direction, the current research works on the prediction of day-ahead wind energy production in island grids, aiming to generate both theoretical (expected) and actual wind power forecasts. To that end, we use artificial neural networks for the development of different day-ahead forecasting models of hourly granularity, and we then test their performance in a large-scale non-interconnected island system, where annual wind energy curtailments for local wind parks may exceed 25% of the respective theoretical yield. Our results indicate that models developed provide a fair accuracy of day-ahead wind energy predictions, which is further elaborated by initiating a discussion on the emergence of alternative actor schemes in similar systems.

Keywords: artificial neural networks; day-ahead forecasting; wind power dispatching; wind energy curtailments; island systems



Citation: Moustris, K.; Zafirakis, D. Day-Ahead Forecasting of the Theoretical and Actual Wind Power Generation in Energy-Constrained Island Systems. *Energies* **2023**, *16*, 4562. <https://doi.org/10.3390/en16124562>

Academic Editor: Adrian Ilinca and Wei-Hsin Chen

Received: 22 March 2023

Revised: 9 May 2023

Accepted: 26 May 2023

Published: 7 June 2023



Copyright: © 2023 by the authors. Licensee MDPI, Basel, Switzerland. This article is an open access article distributed under the terms and conditions of the Creative Commons Attribution (CC BY) license (<https://creativecommons.org/licenses/by/4.0/>).

1. Introduction

Island energy systems are often seen as test beds for novel technological solutions [1], which in turn allows for the early evaluation of relevant merits and challenges in view of their application at a greater scale. A similar course has been followed in the case of wind energy [2], with many island regions determined by high-quality wind potential nowadays exhibiting significant wind energy capacity. This, however, may cause stresses in local energy systems, especially in islands where the variation of load demand presents high levels of seasonality [3,4], mainly due to their touristic character. In more detail and owing to the non-dispatchable character of wind power, it is oftentimes that, under such conditions, local wind parks are faced with increased energy curtailments [5].

To address similar challenges, island energy systems need to become more flexible. Towards this direction, different solutions have gained maturity in recent years. While energy storage technologies remain at the forefront [6–9], new flexibility options emerge, such as with demand response [10,11] and, in a broader sense, advanced energy management. This strongly relates to the progress met in the fields of artificial intelligence and data sciences, enabling the development of advanced forecasting techniques that could be of support in improving dispatching terms of wind power.

To that end, artificial intelligence and, more precisely, artificial neural networks (ANNs) are currently used in the wind energy sector, helping to address aspects in both the design and operation stages of different wind energy applications [12,13]. Interest in the integration of artificial intelligence in the sector is also reflected in the recent body of scientific literature, with emphasis put on the prediction of wind power generation for different time horizons [14,15], as well as on other aspects, such as the predictive maintenance of wind turbines [16].

Development of optimal wind power forecasting models to that end is not strictly limited by the need to generate high-accuracy predictions of the wind power component, or, as Wahndany et al. [17] put it, “a more or less conservative forecast may be preferred over pure accuracy”. Instead, the development of optimal models may extend to also incorporate additional aspects, such as the operational requirements of wider system boundaries and the interplay of different components, aiming to serve the purpose of overarching optimization objectives at the system level. Similar research is topical in the area of wind-based microgrids [18–22], where wind energy penetration is considerable and where the output of wind power forecasting models is used to inform the operation of advanced energy management systems.

In relation to the above and with the goal to further advance research in the field, the present study focuses on settings of energy-constrained island systems that are determined by high shares of wind energy and the experience of significant wind energy curtailments. More specifically, our research offers a new viewpoint on the exploitation of wind power forecasting, with the aim to address aspects of interest not only to system operators, but also to wind energy actors locally involved. With that in mind, we put forward the design, development, and performance evaluation of ANN models for the day-ahead prediction of the theoretical (expected) and actual (dispatched) wind power and proceed to a broader analysis on the interpretation of results obtained towards their meaningful exploitation in the framework of day-ahead dispatch scheduling in similar systems.

To that end, in Section 2 of the paper, we present the relevant input data and provide the problem definition, methods, and performance metrics, focusing on the design of ANN models for the hourly, day-ahead prediction of wind power. Accordingly, in Section 3, we provide the main results of our research and proceed further with their analysis on the basis of a post-processing exercise, seeking to introduce a meaningful interpretation in relation to the requirements of day-ahead dispatch scheduling in energy-constrained island systems. Next, Section 4 discusses the broader meaning of the theoretical and actual wind power forecasting in similar systems, elaborating on the emergence of new actor schemes and markets locally, while Section 5 provides the main conclusions of our research.

2. Materials and Methods

2.1. Input Data

For the purpose of our analysis, we use the Aegean Archipelagos as the study area and apply our methodology for the non-interconnected island system of Kos and Kalymnos. The latter is found in the SE region of the Aegean and comprises nine electrically interconnected islands. The local electricity system features a peak demand of ~105 MW and an annual consumption of ~360 GWh, and hosts a total of four wind parks. These are determined by a total capacity of 15.2 MW and, owing to the limited flexibility locally, are set to face energy curtailments that even exceed 25% of the respective theoretical energy yield on an annual basis [5]. Input data used for our analysis include detailed, hourly estimations of the wind capacity factor (CF) for each of the four wind parks examined and for a time period of two years (2019–2020), arguing that, with the use of the wind power CF as the main feature of our predictions, we are able to better harvest spatial correlation between the examined wind parks' specific energy performance, effectively addressing any impact of unscaled input variables (different power generation scales).

In this context, we estimate two different expressions of wind power CF : the theoretical and the actual one (see also Equations (1) and (2), with E_{theor} and E_{actual} standing as the

theoretical and actual (or absorbed by the grid) output of wind energy over a period of Δt , and with N_o being the operational capacity of the wind park). Estimated time series of the theoretical wind power CF are generated with the use of open wind speed datasets, available from the MERRA2 database [23]. These are properly adjusted to the hub height of installed wind turbines for each of the examined wind parks (see also Table 1), which allows for the estimation of the anticipated, ex ante CF . In the same context, wind power curves of the given wind turbines are also used (Figure 1a), considering at the same time the maximum permitted (licensed) wind power output at the wind park level, with the respective time series firstly generated at the level of each different wind park (Figure 1b).

$$CF_{th} = \frac{E_{theor}}{N_o \cdot \Delta t} \quad (1)$$

$$CF_{act} = \frac{E_{actual}}{N_o \cdot \Delta t} \quad (2)$$

Table 1. Technical characteristics and coordinates of the examined wind parks.

WP	Long.	Lat.	WT	Hub Height	WT (kW)	WT No	WP (kW)
Kos-1	36.747	26.936	Bonus-600	50	600	7	4000
Kos-2	36.753	26.931	Enercon E-40	50	600	6	3600
Kos-3	36.826	27.161	Enercon E-44	55	900	5	3600
Leros	37.160	26.805	Bonus-600	50	600	7	4000

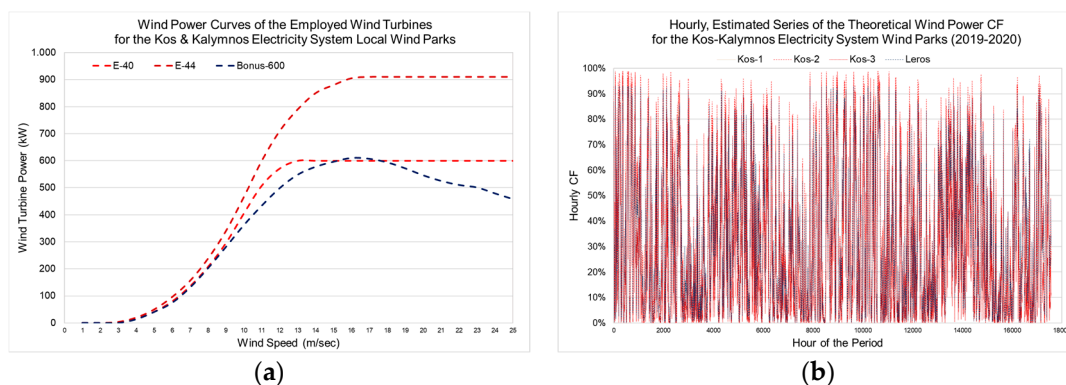


Figure 1. Wind turbines' power curves (a) and theoretical CF time series per wind park (b).

On the other hand, estimation of the actual, ex post wind power CF is based on aggregate wind power generation data provided by the local Distribution System Operator (DSO) over the same time period (i.e., two consecutive years: 2019–2020). Estimation of the actual wind power CF to that end captures in situ, layout-related efficiency characteristics of the examined wind parks, as well as aspects such as wind turbines' downtime periods and periods of wind energy curtailments for the purpose of grid decongestion. Thus, it may provide wind actors with useful information for the investigation of relevant hedging strategies and the recovery of wind energy curtailments. Accordingly, and in Figure 2, the aggregate, weighed output of the four wind parks is compared against the respective actual wind power CF values for the Kos and Kalymnos system, with the 480-h comparison (Figure 2b) designating a very similar trend and revealing a positive difference between the theoretical and actual wind power CF .

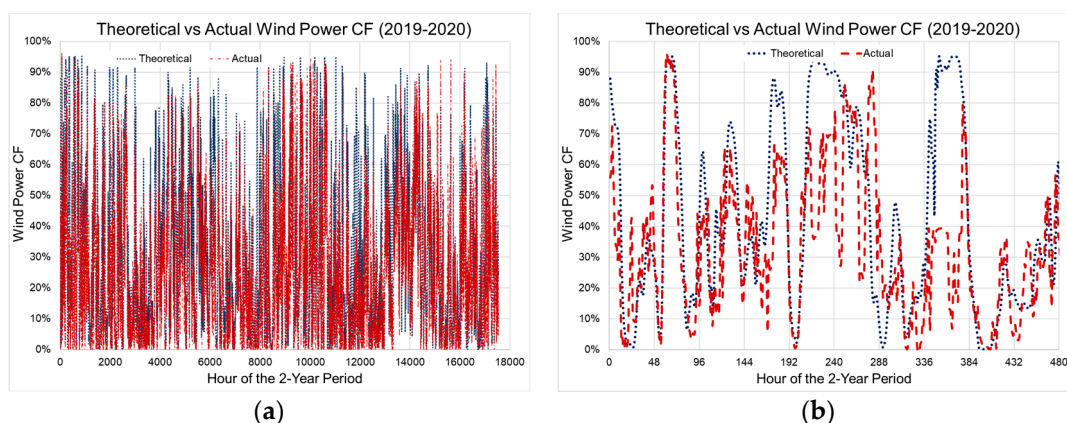


Figure 2. Theoretical vs. actual wind power CF; 2-year period (a) and 20-day instance (b).

The latter is also reflected in Figure 3a, and is explanatory of wind energy curtailments occurring in the local system, with the overall 2-year period CF for the theoretical and actual series, being equal to 32.5% and 23.7%, respectively. Finally, and in Figure 3b, we also present probability density distributions in relation to different wind power CF classes for both the theoretical and actual CF series, with the comparison between the two patterns again suggesting the occurrence of extended curtailments in the local energy system.

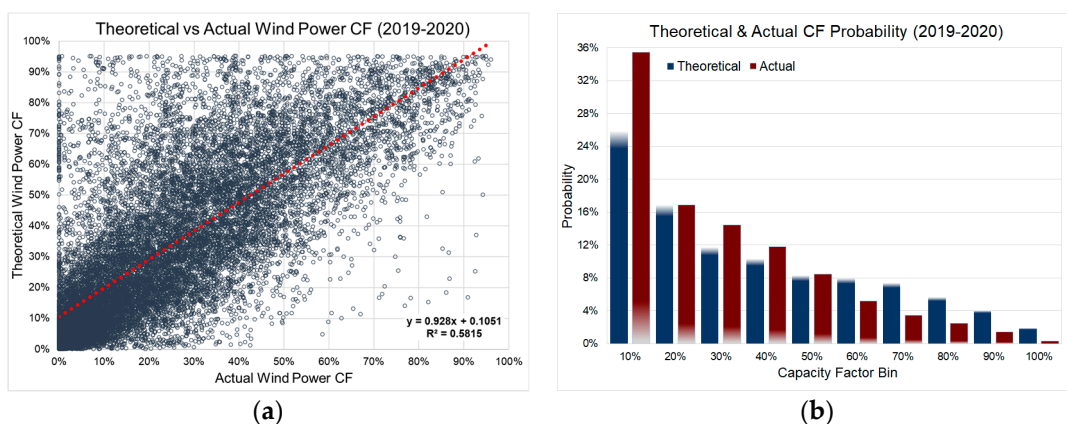


Figure 3. Linear regression (a) and probability density (b) of theoretical vs. actual wind power CF.

2.2. Problem Definition and Methods

In order to produce day-ahead predictions of the theoretical and actual wind power generation on an hourly basis, we proceeded to the development of several ANN models, capturing different types and also architectures of ANNs. The different types of ANNs considered include time-lagged recurrent networks (TLRNs), multilayer perceptron (MLP), and general feed-forward networks (GFFNs). At the same time, different architectures were tested on the basis of a trial-and-error method, under which we evaluated a total of 15 main models for the prediction of the theoretical wind power CF, applying different training algorithms, features, sets of hidden layers and also numbers of input/hidden layers' neurons. In this context, out of the different ANN models examined per different types of ANNs, we excluded the models that were found to be sub-optimal in terms of either accuracy or time complexity, and currently present the results for a subset of four models. The latter includes three adequately performing models (one for each type of ANNs studied), as well as a fourth, best-performing model, that is also applied in the prediction of the actual wind power CF accordingly.

With regard to the development of the models, training parameters taken into account consider input deriving from the previous five days (D-1, D2, D-3, D-4, and D-5), with the aim to provide a total of 24 distinct hourly predictions for the day ahead (D+1). In that way,

the required input for the models' execution becomes independent of data associated with day (D-0). As a result, and in the context of a rolling, day-ahead (D+1) scheduling pattern, increased flexibility is provided concerning the models' execution time over the previous day (D-0). This is considered fundamental for the development of the models, allowing for the incorporation of new, rolling historical data of each (D-1) day, normally cleared and published every other (D-0) day (i.e., one day after). A reasonable assumption to that end is that the selected model is executed at 12:00 of day (D-0), allowing for the incorporation of (D-1) data on the one hand and for the delivery of forecasting results in view of configuring the day-ahead dispatching schedule on the other.

With this in mind, in Table 2, we present the inputs used for the training of the given ANN models, together with the respective generated output. In more detail, and as already seen, out of the initial set of developed models, a total of four models are currently presented, with the fourth model also capturing additional input parameters, which are highlighted in Table 2 (in grey). To that end, the first three models exploit a total of 28 inputs, forming an input layer of 28 artificial neurons, while the fourth one considers 38 inputs and, thus, an input layer of 38 neurons, with the overall aim being to generate a model of both increased accuracy and of a wide prediction span regarding different CF classes (see also Section 3.1).

Table 2. Training input and output of the developed ANN models.

Input/Training Data	Model No	Output
Number of month (1–12) for D-1, D-2, D-3, D-4, and D-5	1–4	The hourly wind power CF (theoretical or actual) for each given hour of D + 1 (24 values)
Number of day (1–31) for D-1, D-2, D-3, D-4, and D-5		
Number of hour (1–24) for D-1, D-2, D-3, D-4, and D-5		
Theoretical CF, for the given prediction hour (H), for D-1 to D-5		
Actual CF, for the given prediction hour (H), for D-1 to D-5		
Number of month (1–12) for D + 1		
Number of day (1–31) for D + 1	4	
Number of hour (1–24) for D + 1		
<i>Max CF of the last 12 h before prediction hour (H), for D-1 to D-5</i>		
<i>Min CF of the last 12 h before prediction hour (H), for D-1 to D-5</i>		

- **Model 1:** The first model developed is a time-lagged recurrent network (TLRN) model [24–26]. It comprises a 28-neuron input layer and is combined with a 4-neuron hidden layer and a single-neuron output layer, using the back-propagation training algorithm and the activation function of tanhaxon.
- **Model 2:** The second model developed is a multilayer perceptron (MLP) ANN model [27,28], which, in addition to the 28-neuron input layer, also carries one hidden layer of 24 neurons and an output layer of a single neuron. Moreover, it uses the same training algorithm and the same activation function as the TLRN model.
- **Model 3:** The third model is a general feed-forward network (GFFN) model [29,30], having the same structure, training algorithm, and activation function as the MLP.
- **Model 4:** The fourth model is also a GFFN model, but with a different structure. More specifically, it also incorporates the max and min CF values of the last 12 h, up to the given prediction hour, considering each of the five previous days and aiming to the generation of predictions both of higher accuracy and for a wider span of wind power CF bins. As such, it employs a total of 38 neurons for the input layer. Moreover, and due to the inclusion of extra features, it comprises two hidden layers, with 35 and 17 neurons, respectively, and has an output layer of a single neuron (see also Figure 4).

The activation function applied remains the same as before (tanhaxon), while for the learning rule, we used the gradient descent with momentum.

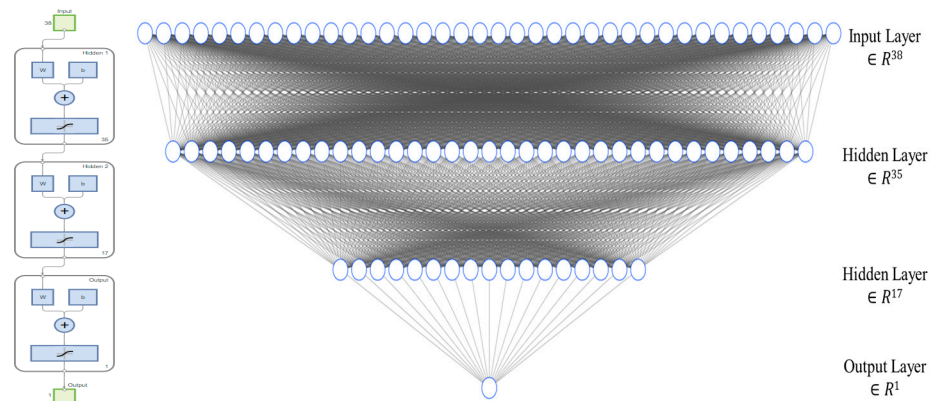


Figure 4. ANN structure of the GFFN-opt model, including an input layer of 38 neurons, two hidden layers of 35 and 17 neurons, and an output layer of 1 neuron.

With regard to the training of the presented models, we used the time series of 2019 and developed two subsets of data. The first subset included 80% of the available training dataset, with the rest 20% of the second subset used for the purpose of cross-validation. The subsets were created randomly, while for the performance evaluation of the models, we used the data series of 2020, not used in the training stage of the models. Finally, training, validation, and also performance evaluation of the models were performed with the support of MATLAB software (ed. MATLAB R2022b).

2.3. Performance Indicators

Concerning the evaluation of the developed ANN models, appropriate statistical performance indicators were used [31,32], such as the correlation coefficient (R), the mean bias error (MBE), the root mean square error ($RMSE$) the index of agreement (IA), and the normalized mean absolute error ($NMAE$), analyzed in the following and represented by the set of Equations (3) to (7), where P_i concerns the predicted values and O_i the corresponding observed values, and where n is the population of predictions (pairs).

$$R = \frac{n \cdot \sum_{i=1}^n P_i \cdot O_i - \sum_{i=1}^n P_i \cdot \sum_{i=1}^n O_i}{\sqrt{n \cdot \sum_{i=1}^n P_i^2 - (\sum_{i=1}^n P_i)^2} \cdot \sqrt{n \cdot \sum_{i=1}^n O_i^2 - (\sum_{i=1}^n O_i)^2}} \quad (3)$$

$$MBE = \frac{1}{n} \sum_{i=1}^n (P_i - O_i) \quad (4)$$

$$RMSE = \sqrt{\frac{1}{n} \sum_{i=1}^n (P_i - O_i)^2} \quad (5)$$

$$IA = 1 - \frac{\sum_{i=1}^n (P_i - O_i)^2}{\sum_{i=1}^n [|P_i - O_{ave}| - |O_i - O_{ave}|]^2} \quad (6)$$

$$NMAE = \frac{1}{n} \sum_{i=1}^n \frac{|P_i - O_i|}{O_{max}} \quad (7)$$

- R measures how strong a relationship is between two variables, in our case, between the predicted and the observed values of CF . Values of R range from -1 to $+1$, with -1 indicating a perfectly linear and negative, i.e., inverse, correlation and $+1$ indicating a perfectly linear and positive correlation. In the case of ANN models' prediction,

the best score of R is 1, indicating that all of the predicted values are equal to the corresponding observed values.

- MBE shows the degree of correspondence between the mean forecast and the mean observation. MBE is used to quantify whether the model underestimates or overestimates the observed data. Positive values indicate an overestimation, and negative values indicate an underestimation.
- $RMSE$ is a quadratic scoring rule that also measures the average magnitude of the error. More concretely, it is the square root of the average of squared differences between predictions and observations. $RMSE$ provides the average of model prediction errors expressed in the units of the variable of interest.
- IA gives a measure of how close the predicted P_i and the observed O_i values are, taking values from 0 to 1. Values of IA close to 1 indicate that the predicted values are close to the observed ones, and as such, a small prognostic error occurs.
- $NMAE$ is the average of the absolute differences between the observed and predicted values, normalized on the maximum measured value, which is currently equal to the max value of CF , i.e., 100%.

Results obtained to that end for the prediction of the theoretical and actual wind power CF for the 24 h day-ahead horizon studied are presented in the following section.

3. Results

3.1. Theoretical CF

Following the training and validation stages for the tested models, their performance was evaluated on the basis of data series from the year 2020, through the application of statistical indicators analyzed previously. Evaluation results obtained to that end concerning the prediction of the theoretical wind power CF are summarized in Table 3, where, as one may note, the second GFFN model (hereafter symbolized with GFFN-opt) comprises the model determined by the best performance across all of the involved metrics. In the same context, and although a direct comparison between different cases cannot be easily achieved, results obtained from other studies in the field indicate similar evaluation metrics for optimal, ANN-based day-ahead wind power prediction models addressing wind power installations of analogous scale (e.g., an $NMAE$ of ~17% is recorded in [33] regarding a wind park of 15.8MW), neglecting at this stage any spatial smoothing effect [34] due to the aggregation of four distinct wind parks in our case.

Table 3. Models' performance evaluation: theoretical CF models.

Model	R	MBE	$RMSE$	IA	$NMAE$
TLRNs	0.106	−0.011	0.264	0.313	0.220
MLP	0.191	−0.031	0.275	0.476	0.222
GFFNs	0.186	−0.029	0.268	0.445	0.219
GFFNs-opt	0.516	−0.030	0.230	0.695	0.179

Returning to the comparison made between the different models examined, this is better reflected in Figure 5a, where a two-week period comparison between the observed and predicted values generated by each of the models is provided for the first two weeks of 2020. As can easily be concluded, the TLRN model captures the average trend of the observed pattern, with the MLP and GFFN models presenting a better and similar behavior that outperforms TLRN. At the same time, the second GFFN model (GFFN-opt) is found to present the best fit, which is justified by the consideration, during the training stage, of the last 12 h maximum and minimum CF values. Furthermore, Figure 5b provides the probability distribution of residuals for each of the models examined, referring to the entire dataset of the year 2020. Residuals refer to the difference between the observed and the predicted values. As such, a positive difference suggests the underestimation of generated

predictions, and a negative one overestimation. In this context, the distribution of the GFNN-opt model appears rather symmetrical around the minus 10% bin, and also narrower, opposite to the case of the other models, peaking close to the residual bin of minus 30% and presenting a wider shape. Actually, beyond the $\pm 30\%$ range, cumulative probability drops to less than 15% for the GFNN-opt model, with the rest of the models presenting higher and more persisting probability values in both the lower and higher residual bins. To that end, it is for all four models that the probability value almost zeroes for residual bins that are lower than minus 70% and higher than 70%, demonstrating that even the least performing ones are able to provide predictions of moderate, but still reasonable accuracy, for the day-ahead time horizon examined.

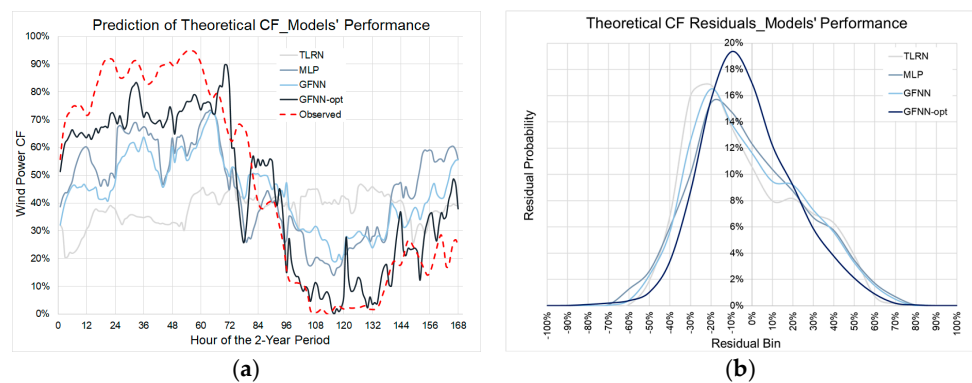


Figure 5. Observed vs. predicted series for a 2-weeks' instance (a) and residuals' probability distribution for year 2020; (b) theoretical CF models.

Moreover, and by also analyzing residuals on the basis of different classes of theoretical wind power CF (Figure 6), the superiority of the GFNN-opt model is again demonstrated.

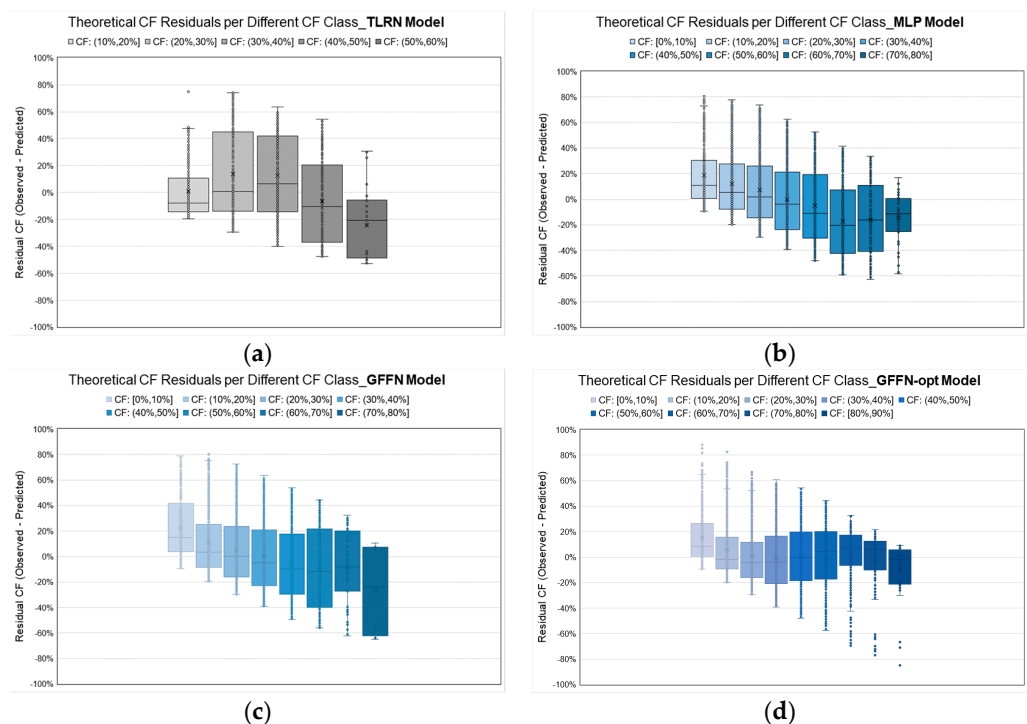


Figure 6. Variation of day-ahead CF residuals per different CF classes: prediction of theoretical wind power CF using the TLRN (a), the MLP (b), the GFNN (c), and the GFNN-opt (d) models.

This is also supported by the fact that the GFFN-opt model captures a wider span of predictions of theoretical wind power *CF* values, which also includes the *CF* class of 80–90%. Meanwhile, the TLRN model is limited in the range of *CF* classes between 10% and 60%, while the GFFN and MLP models, although capturing predictions for *CF* classes reaching 80%, are also outperformed by the GFFN-opt model, especially in the area of higher-order *CF*s.

3.2. Actual vs. Theoretical *CF*

Following the comparison between the performance of the different models concerning the prediction of theoretical *CF* values, we then proceed to compare the performance of the best-fit model (GFNN-opt) with regard to the prediction of the theoretical and actual wind power *CF*. The latter, as already seen, takes into account wind power that is absorbed by the local energy system and thus incorporates instances of wind energy curtailments. Evaluation results on the performance of the GFNN-opt model for the actual *CF* are given in Table 4 against the respective of the theoretical *CF*.

Table 4. Models’ performance evaluation: theoretical and actual *CF* best-fit models.

Model	<i>R</i>	<i>MBE</i>	<i>RMSE</i>	<i>IA</i>	<i>NMAE</i>
GFFNs-opt (theoretical)	0.516	−0.030	0.230	0.695	0.179
GFFNs-opt (actual)	0.239	−0.044	0.228	0.489	0.178

As it may be concluded from the above table, performance of the developed model is more limited in the case of the actual wind power *CF*. At this point, it must be noted that the actual wind power *CF* pattern presents a greater coefficient of variation (87.8%) in relation to the theoretical one (78.8%), which can be explained by the exercise of technical factors, which both limit the levels of *CF* values overall and introduce features of more stochastic character. These factors include grid constraints, such as the dynamic penetration constraint, and operational limitations of involved thermal power generators, associated with the technical characteristics of the thermal fleet, the appearing levels of load demand, and the overarching dispatching strategy adopted by the local DSO. As such, further details would be required in order to adequately describe the influence of these parameters as well.

Acknowledging the above, two different sets of curves are given in Figure 7a, representing the observed and predicted values of the theoretical and actual wind power *CF*, again for the first two weeks of the year 2020. If looking into the resulting trends, the theoretical *CF* model seems to adjust better to the respective observed values.

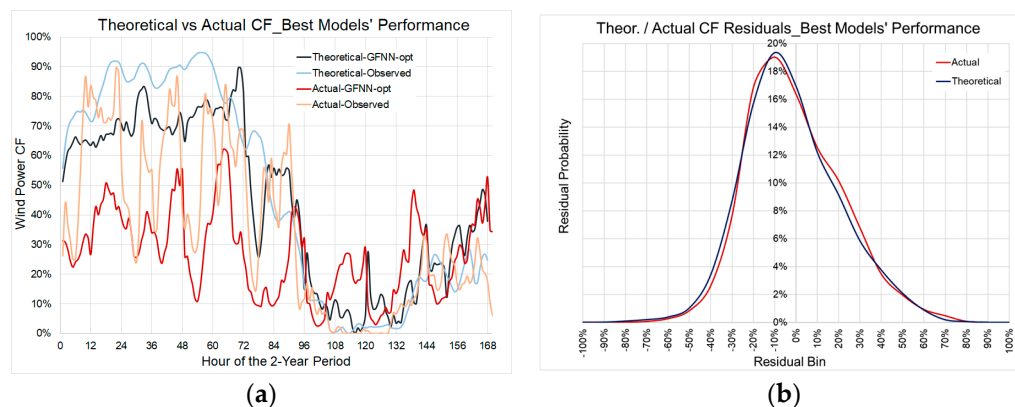


Figure 7. Observed vs. predicted series for a 2-weeks’ instance (a) and residuals’ probability distribution for year 2020; (b) best-fit models for the theoretical and actual *CF*.

On the other hand, and owing to the fact that the actual *CF* series is determined, on average, by values that are ~25% lower than the respective of the theoretical series, the probability distributions of residuals for the two cases are almost identical (Figure 7b).

3.3. Post-Processing and Analysis

Further elaborating on the results obtained, we accordingly proceed with a mapping exercise. The latter aims to provide meaningful post-processing and interpretation that may enable informed decision making regarding the day-ahead dispatch scheduling of power generation assets in similar, energy-constrained island systems, determined by high shares of wind energy and also the experience of increased wind energy curtailments for local wind energy actors.

3.3.1. Residuals' Matrices

Acknowledging the above, first, we create different *CF* classes (predicted values) and assess the range of anticipated residuals per different classes and hours of the day. In that way, predictions generated are also defined by the range of residuals attributed to the given hour and class of *CF*, thus offering the potential for the introduction of probabilistic signals concerning wind power forecasting. Two different matrices are developed to that end. The first concerns the prediction of the theoretical wind power *CF* (Figure 8) and the second prediction of the actual wind power *CF* (Figure 9).

As far as the first matrix is concerned, it can be seen that in the range of $0\% < CF < 20\%$, predictions generated tend to underestimate the observed values, while the opposite is valid for *CF* values kept higher than 50–60%. At the same time, the greater (absolute) residual values are noted for the higher *CF* bins (>70%), where overestimation of observed values may even reach 80%. On the other hand, pronounced overestimation in the case of actual wind power *CF* (Figure 9) presents itself for values greater than 40%, while classes of *CF* higher than 80% are not made available, since *CF* predictions generated remain below 80%, even in the case of observed values reaching 100%. As can be seen (Figure 8), the same is valid in the case of the theoretical wind power *CF* as well, with prediction results this time limited by a ceiling value of 90%.

In addition to the box plot analysis provided in the previous figures, we next proceed to the synthetic presentation of residuals per different *CF* classes and hours of the day. We do so indicatively for the 25th, the 50th, and the 75th percentiles of residuals, and in the form of heatmaps presented in Figure 10.

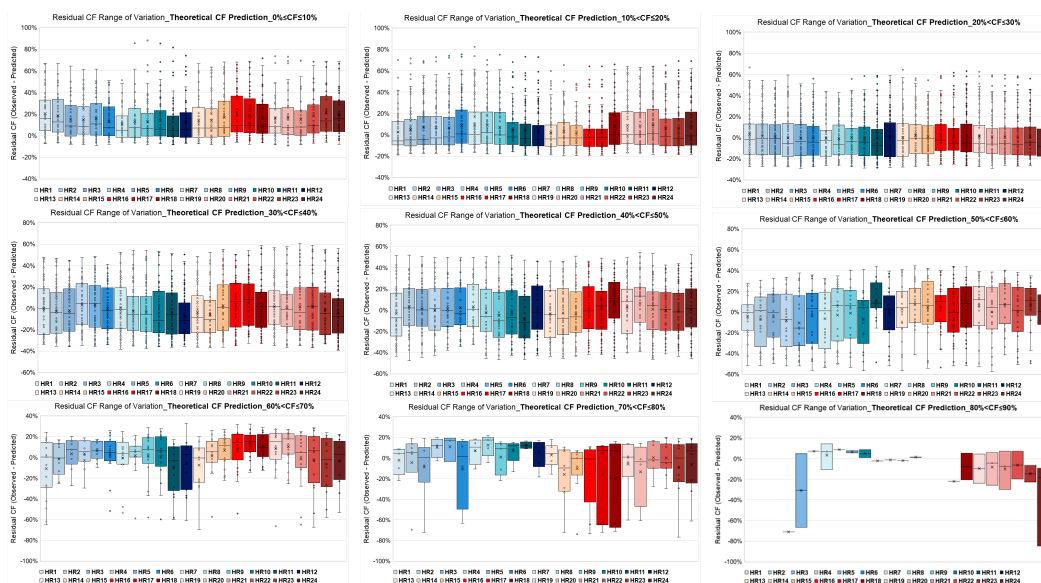


Figure 8. Hourly variation of day-ahead *CF* residuals, per *CF* class: theoretical *CF* prediction.

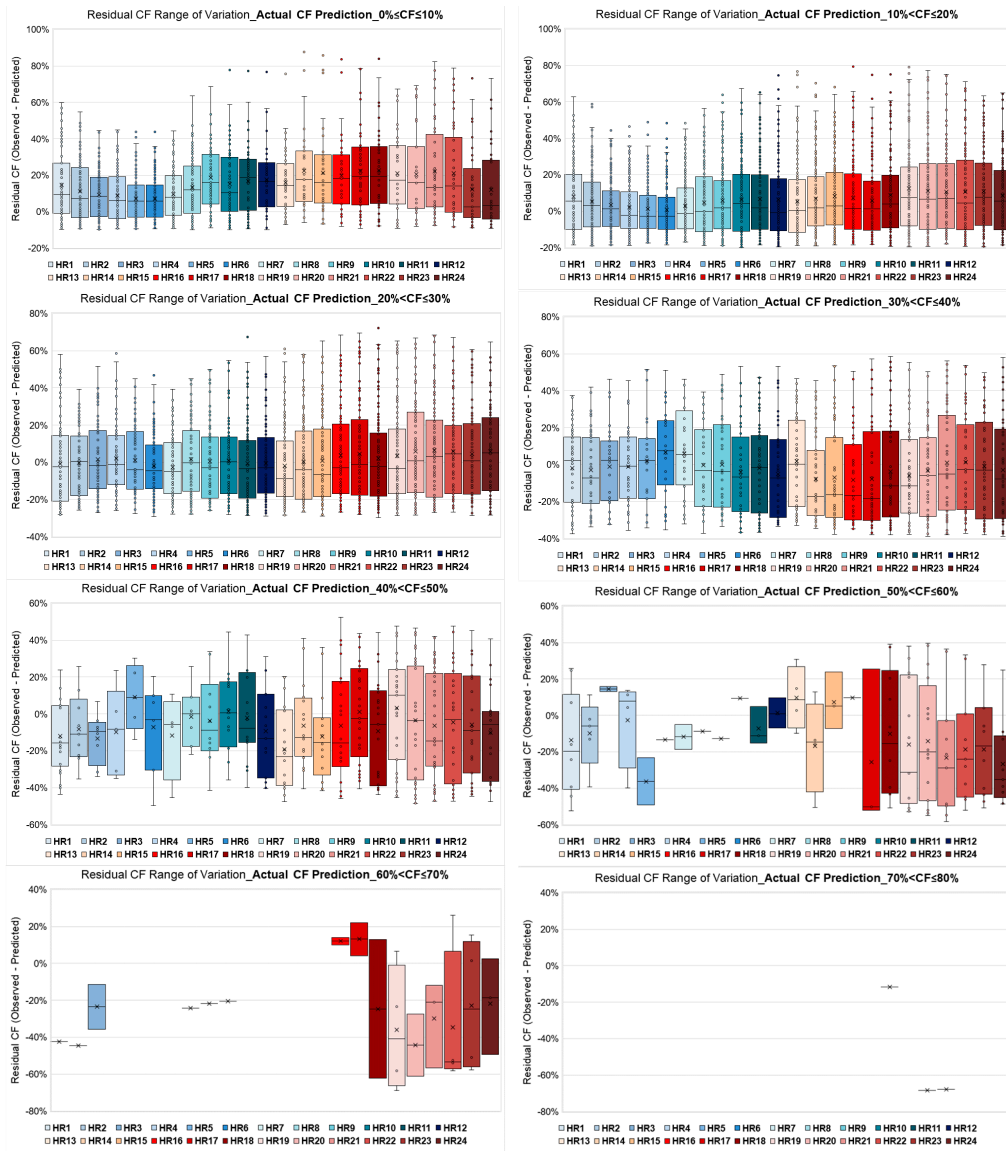


Figure 9. Hourly variation of day-ahead CF residuals, per CF class: actual CF prediction.

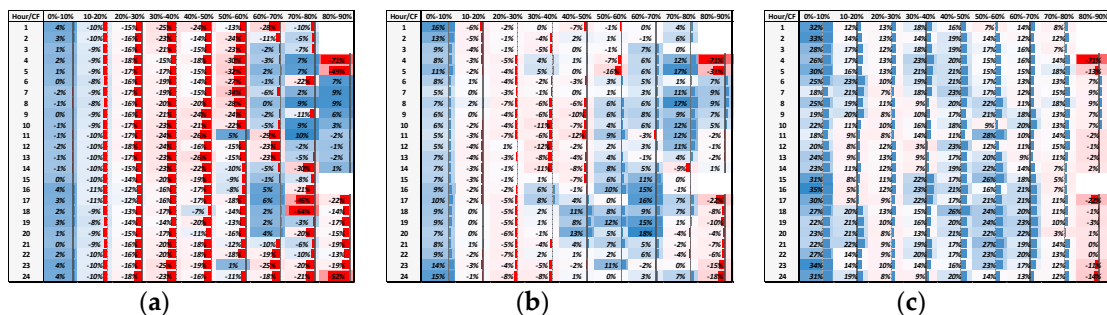


Figure 10. Cont.

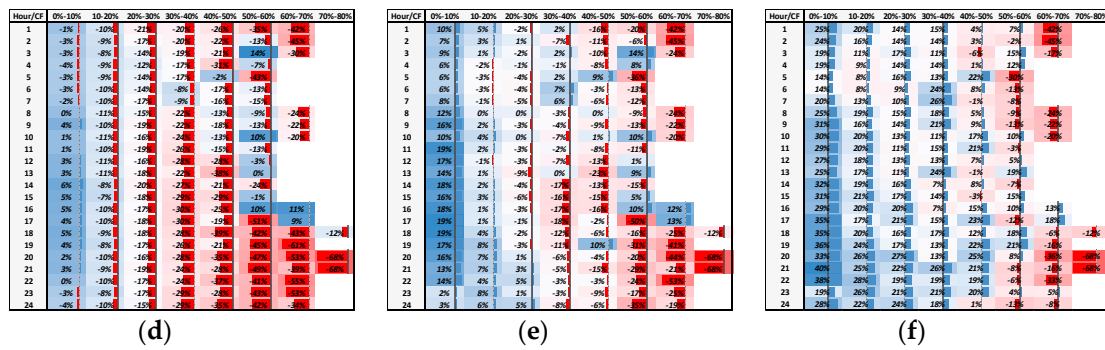


Figure 10. Heatmaps of theoretical & actual CF prediction residuals: p25 (a,d), p50 (b,e), & p75 (c,f).

According to the heatmaps, significant underestimation is noted in the lower ranges of CF values, and for the higher percentiles (50th and 75th), for both the theoretical and actual wind power CF predictions, especially for CF values below 20%. At the same time, and as already seen, actual CF predictions appear to be overestimating the respective observed values of higher CF, in a rather pronounced way and for CF values exceeding 40–50%.

3.3.2. Residuals' Weights

Accordingly, by considering the annual probability distributions for the predicted values of the theoretical and actual CF, per class of CF and per hour of the day, different classes of predictions carry different probability weights on an annual basis (Figure 11). For example, although overestimation with regard to the observed, actual wind power CF values falling in the range of 70–80% even reaches ~68%, the probability of encountering similar predictions is almost zero.

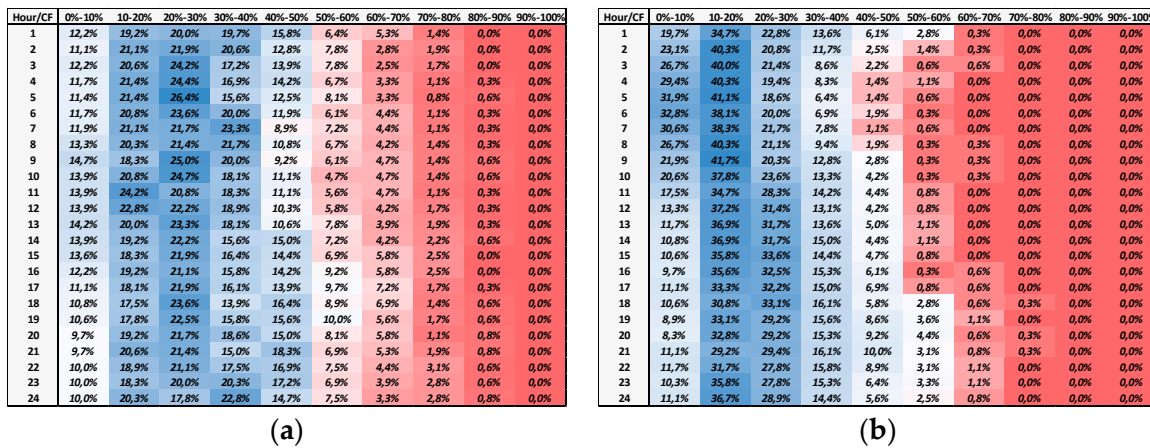


Figure 11. Annual probability heatmaps of theoretical (a) & actual (b) CF prediction classes.

Arguing to that end that the weight of residuals estimated should also factor in the annual probability of encountering a given CF prediction class, the heatmaps of Figure 10 are accordingly rebuilt (Figure 12), using the product of residual percentiles' and predictions' probabilities. The latter is currently assumed to better represent the significance of each given residual, per different day hours and CF bins, which, as expected, causes the weights of the residuals to strengthen for the lower of CF bins, weakening them for the higher ones.

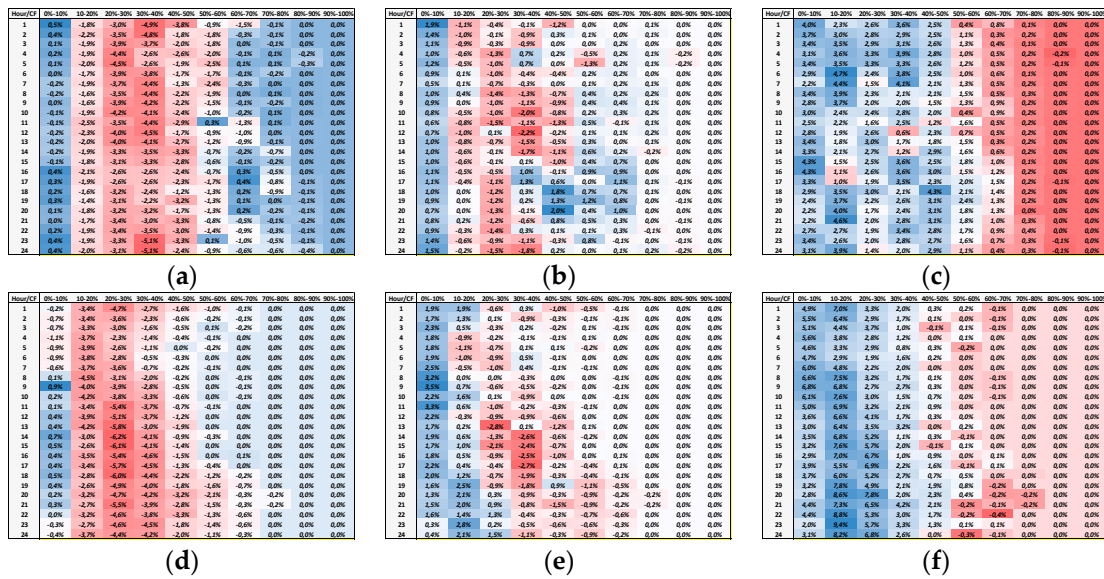


Figure 12. Heatmaps of theoretical & actual CF residuals' weight: p25 (a,d), p50 (b,e), & p75 (c,f).

3.3.3. Analysis per Class of CF and Day-Ahead Hours

A more abstract view of results is provided in Figures 13 and 14, where the average weights of residuals per different CF classes and day hours are provided. Average values are estimated on the basis of heatmaps given in Figure 12 (per column and row, respectively), while the weight of residuals is provided in a normalized fashion, relative to the maximum absolute value for each different (25th, 50th, and 75th percentiles) pair of theoretical and actual heatmaps. According to Figure 12, the relative weight of residuals appears more important in the case of the actual CF for CF values up to 30%. On the other hand, for CF values exceeding 60%, the relative weight of residuals zeroes, owing to the annual probability attached to the respective predictions (Figure 12b).

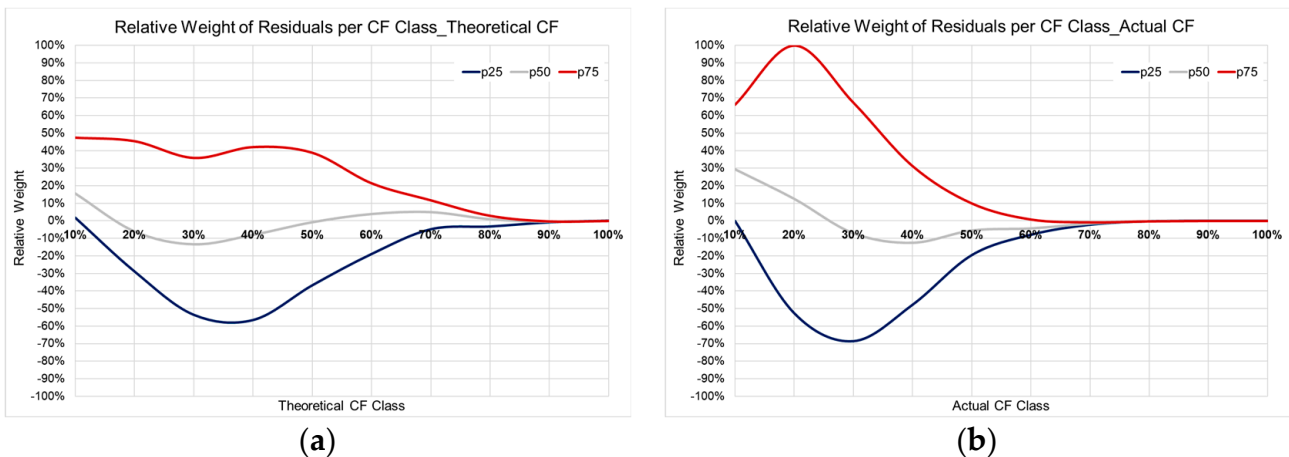


Figure 13. Normalized weight of residuals per different CF bins and percentiles for the theoretical (a) and the actual (b) CF.

becomes more important between 20:00 pm and 24:00 pm for the actual CF, and less important between 10:00 am and 14:00 pm for the theoretical CF.

In the meantime, and in relation to the post-processing analysis of the prediction results, it can also be inferred that decision making on the selection of best-performance models should not be restricted to the results of evaluation metrics covering the entire problem space alone (see also Table 3); rather, it can also relate to specific application needs, narrower problem spaces, and also to the weight of importance assigned to different classes of results (see also Figure 15). In this context, and although not in the core scope of the present study, parallel exploitation of different models under this view may also add to the analysis towards the direction of ensemble modeling [35].

Average Residuals of ANN Models_Theoretical CF_30%<CF≤40%

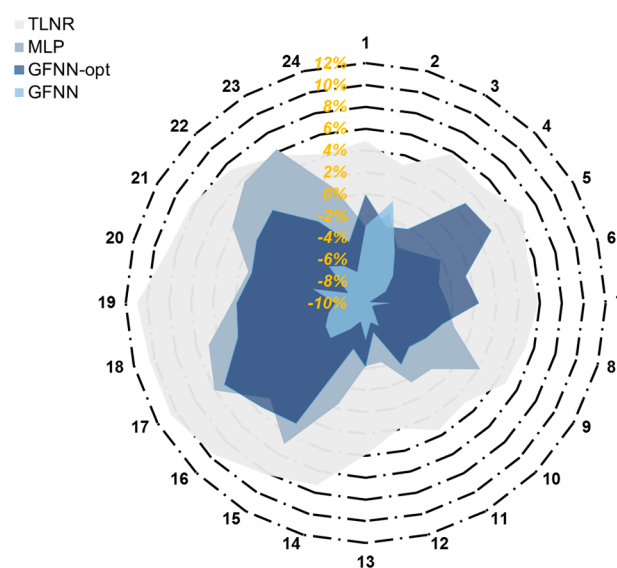


Figure 15. Average values of residuals for the examined set of ANN models and the theoretical CF bin of 20–30%.

Having said that, results provided in the previous, exemplary Figure 15 gather the residuals of theoretical wind power CF predictions for a certain range of CF prediction values (between 20% and 30%) and for all four ANN models currently examined, indicating that independently of their overall performance scores (see also Table 3 and Figure 4), different models may find themselves outperforming one another at a lower level of analysis, for which performance per different hours of the day is also taken into account.

4. Discussion

Following the analysis of results, we currently place our arguments on their meaningful character for both local system operators and wind energy actors.

The measured ability to predict the theoretical, hourly day-ahead wind power generation CF, appreciating at the same time a fair estimation of the respective CF residuals' probability, provides local system operators with sufficient information in order to proceed to relevant decision making concerning day-ahead dispatching schedules, aiming to the maximization of absorbed wind energy by the local, island energy systems and to the minimization of system costs. Moreover, since the corresponding results may be generated at any point of the day (D-0), being dependent only on values deriving from days (D-1) to (D-5), sufficient flexibility is also provided to island system operators in terms of execution time for the selected models.

To that end, and given also the accuracy levels of optimum forecasting models developed, a considerable reduction of spinning reserve requirements is also possible for local system operators, which in turn reduces system operational costs. At this point, it is im-

portant to mention that in energy-constrained island systems, where, as anticipated, wind farms are geographically concentrated, the rule of thumb for the determination of spinning reserve requirements concerning the component of wind power generation assumes, in the absence of reliable predictions, a rather moderate guaranteed share of wind power generation that varies, depending on the island system examined, between 0% and 20% of the respective wind capacity [36].

Furthermore, the ability to predict the actual wind power CF is of added value concerning the design and valuation of dedicated storage systems, used for the recovery of wind energy curtailments. Such storage entities may be seen as a means of transforming existing wind parks into dispatchable units, which introduces different working schemes. The latter may comprise a single actor (coupled wind and storage with common coupling), multiple actors, or independent actors. In the last two scenarios, centralized storage that may stand as either a completely independent entity or an asset that is co-owned by multiple wind actors implies the prospect of partial storage leasing on the one hand and of cooperative models on the other. Further on, under the prospect of looking at an independent, centralized storage entity, day-ahead forecasting of actual and theoretical wind power could inform price offers of wind actors on the commitment of, e.g., daily storage capacity shares, building also on the establishment of a similar, local-scale market between wind power and storage actors. The same is of course valid for the case of emerging demand response services, with relevant assets broadening the context of such markets and, thus, increasing competition.

Finally, and as far as forecasting results are concerned, further work in the given area could address ensemble modeling as well as the development of additional models, e.g., on a seasonal basis, that could better capture long-term, daily changes in the patterns of wind power generation and especially in those of the actual wind power CF . Moreover, the same is also valid for clustering-based forecasting, with a more detailed time series pre-processing potentially leading to the generation of more meaningful model features. At the same time, the development of wind park level, rather than system-level forecasting models, adds to the discussion of hedging strategies for existing and future wind park actors, allowing also for a comparative evaluation of local and aggregate-scale wind power forecasting.

5. Conclusions

In the present study, we examined the problem of day-ahead wind power forecasting in the context of saturated, in terms of wind power capacity, island electricity systems. Using ANNs, we developed and evaluated different day-ahead models for the hourly prediction of the theoretical and actual wind power CF in a given island system of the Aegean Sea, arguing that such prediction signals are of importance for both the local DSOs and wind park actors. Next, we proceeded with a post-processing of results. The latter focused on the analysis of prediction residuals with the aim of generating an extensive map for informing probabilistic decision making of day-ahead dispatch scheduling in similar island systems, looking also into the significance (probability of occurrence) of different scale residuals, projected to the dimensions of CF class and day-time hours. At the same time, optimal ANN models developed provided a fairly good accuracy over the biggest span of CF values for both the theoretical and actual wind power CF , allowing at the same time for a (D-0)-independent model execution, which adds considerably in terms of operational flexibility. Finally, in the context of a broader interpretation of the research output, exploitation of results was discussed, with an outlook on the emergence of local-scale markets and new actor schemes in similar, energy-constrained island systems.

Author Contributions: K.M.: Conceptualization, methodology, data curation, software, validation, writing—review and editing. D.Z.: Conceptualization, methodology, resources, data curation, visualization, formal analysis, writing—original draft. All authors have read and agreed to the published version of the manuscript.

Funding: This research has been co-financed by the European Union and Greek national funds through the Operational Program Competitiveness, Entrepreneurship and Innovation, under the call RESEARCH—CREATE—INNOVATE (project code: T2EDK-01578)



Co-financed by Greece and the European Union

Data Availability Statement: Wind data were retrieved from the open database MERRA-2, through the online tool Renewables.ninja—<https://www.renewables.ninja> (accessed on 10 March 2023). Moreover, aggregate, actual wind power time series were provided by the Hellenic Electricity Distribution Network Operator, in the context of annual report documents under the title “Technical & Economic Data of the Autonomous Power System of Kos and Kalymnos” for years 2020–2021.

Conflicts of Interest: The authors declare no conflict of interest.

References

- Katsaprakakis, D.A.; Proka, A.; Zafirakis, D.; Damasiotis, M.; Kotsampopoulos, P.; Hatziargyriou, N.; Dakanali, E.; Arnautakis, G.; Xevgenos, D. Greek Islands’ Energy Transition: From Lighthouse Projects to the Emergence of Energy Communities. *Energies* **2022**, *15*, 5996. [CrossRef]
- Monteiro Alves, L.M.; Costa, A.L.; Carvalho, M.G. Analysis of potential for market penetration of renewable energy technologies in peripheral islands. *Renew. Energy* **2000**, *19*, 311–317. [CrossRef]
- Tzanes, G.; Zafirakis, D.; Makropoulos, C.; Stamou, A.; Kaldellis, J.K. Energy vulnerability and the exercise of a data-driven analysis protocol: A comparative assessment on power generation aspects for the non-interconnected islands of Greece. *Energy Policy* **2023**, *177*, 113515. [CrossRef]
- Notton, G.; Duchaud, J.L.; Nivet, M.L.; Voyant, C.; Chalvatzis, K.; Fouilloy, A. The electrical energy situation of French islands and focus on the Corsican situation. *Renew. Energy* **2019**, *135*, 1157–1165. [CrossRef]
- Kaldellis, J.K.; Tzanes, G.T.; Papapostolou, C.; Kavadias, K.; Zafirakis, D. Analyzing the Limitations of Vast Wind Energy Contribution in Remote Island Networks of the Aegean Sea Archipelagos. *Energy Procedia* **2017**, *142*, 787–792. [CrossRef]
- Latorre, F.J.G.; Quintana, J.J.; De la Nuez, I. Technical and economic evaluation of the integration of a wind-hydro system in El Hierro island. *Renew. Energy* **2019**, *134*, 186–193. [CrossRef]
- Katsaprakakis, D.A.; Voumvoulakis, M. A hybrid power plant towards 100% energy autonomy for the island of Sifnos, Greece. Perspectives created from energy cooperatives. *Energy* **2018**, *161*, 680–698. [CrossRef]
- Kaldellis, J.K.; Zafirakis, D. Prospects and challenges for clean energy in European Islands. The TILOS paradigm. *Renew. Energy* **2020**, *145*, 2489–2502. [CrossRef]
- Bakos, G.C. Feasibility study of a hybrid wind/hydro power-system for low-cost electricity production. *Appl. Energy* **2002**, *72*, 599–608. [CrossRef]
- Stathopoulos, M.; Zafirakis, D.; Kavadias, K.; Kaldellis, J.K. The Role of Residential Load-management in the Support of RES-Based Power Generation in Remote Electricity Grids. *Energy Procedia* **2014**, *46*, 281–286. [CrossRef]
- Sarmas, E.; Spiliotis, E.; Marinakis, V.; Tzanes, G.; Kaldellis, J.K.; Doukas, H. ML-based energy management of water pumping systems for the application of peak shaving in small-scale islands. *Sustain. Cities Soc.* **2022**, *82*, 103873. [CrossRef]
- Noman, A.A.; Tasneem, Z.; Sahed, M.F.; Muyeen, S.M.; Das, S.K.; Alam, F. Towards next generation Savonius wind turbine: Artificial intelligence in blade design trends and framework. *Renew. Sustain. Energy Rev.* **2022**, *168*, 112531. [CrossRef]
- Wang, Y.; Zou, R.; Liu, F.; Zhang, L.; Liu, Q. A review of wind speed and wind power forecasting with deep neural networks. *Appl. Energy* **2021**, *304*, 117766. [CrossRef]
- Yin, R.; Li, D.; Wang, W.; Chen, W. Forecasting method of monthly wind power generation based on climate model and long short-term memory neural network. *Glob. Energy Interconnect.* **2020**, *3*, 571–576. [CrossRef]
- Rodríguez, F.; Florez-Tapia, A.M.; Fontán, L.; Galarza, A. Very short-term wind power density forecasting through artificial neural networks for microgrid control. *Renew. Energy* **2020**, *145*, 1517–1527. [CrossRef]
- Seongpil, C.; Minjoo, C.; Zhen, G.; Torgeir, M. Fault detection and diagnosis of a blade pitch system in a floating wind turbine based on Kalman filters and artificial neural networks. *Renew. Energy* **2021**, *169*, 1–13.
- Wahdany, D.; Schmitt, C.; Cremer, J.L. More than accuracy: End-to-end wind power forecasting that optimises the energy system. *Electr. Power Syst. Res.* **2023**, *221*, 109384. [CrossRef]
- Weichao, D.; Hexu, S.; Chunxiao, M.; Zheng, L.; Jingxuan, Z.; Huifang, Y. Forecast-driven stochastic optimization scheduling of an energy management system for an isolated hydrogen microgrid. *Energy Convers. Manag.* **2023**, *277*, 116640.
- Silva, D.P.; Salles, J.L.F.; Fardin, J.F.; Rocha Pereira, M.M. Management of an island and grid-connected microgrid using hybrid economic model predictive control with weather data. *Appl. Energy* **2020**, *278*, 115581. [CrossRef]
- Silva, D.P.; Salles, J.L.F.; Fardin, J.F.; Rocha Pereira, M.M.; Ottz, V.C.; Da Silva, F.B.B.; Pignaton, E.G. Measured and forecasted weather and power dataset for management of an island and grid-connected microgrid. *Data Br.* **2021**, *39*, 107513. [CrossRef]

21. Yousri, D.; Farag, H.A.Z.; Zeineldin, H.; El-Saadany, E.F. Integrated model for optimal energy management and demand response of microgrids considering hybrid hydrogen-battery storage systems. *Energy Convers. Manag.* **2023**, *280*, 116809. [[CrossRef](#)]
22. Sizhou, S.; Chenxi, W.; Yu, W.; Xuehua, Z.; Huacai, L. Multi-objective optimization dispatching of a micro-grid considering uncertainty in wind power forecasting. *Energy Rep.* **2022**, *8*, 2859–2874.
23. Gelaro, R.; Coauthors. The Modern-Era Retrospective Analysis for Research and Applications, Version 2 (MERRA-2). *J. Clim.* **2017**, *30*, 5419–5454. [[CrossRef](#)]
24. Wang, Y.M.; Seydou, T. Time-lagged recurrent network for forecasting episodic event suspended sediment load in typhoon prone area. *Int. J. Phys. Sci.* **2009**, *4*, 519–528.
25. Manabendra, S.; Bhattacharjya, R.K. Geomorphology-based Time-lagged Recurrent Neural Networks for Runoff Forecasting. *J. Civ. Eng.* **2012**, *16*, 862–869.
26. Girish, K.J.; Kanchan, S. Time-delay neural networks for time series prediction: An application to the monthly wholesale price of oilseeds in India. *Neural Comput. Appl.* **2014**, *24*, 563–571.
27. Taghinezhad, J.; Sheidaei, S. Prediction of operating parameters and output power of ducted wind turbine using artificial neural networks. *Energy Rep.* **2022**, *8*, 3085–3095. [[CrossRef](#)]
28. Wang, H.; Wang, J. Short-term wind speed prediction based on feature extraction with Multi-task Lasso and Multilayer Perceptron. *Energy Rep.* **2022**, *8*, 191–199. [[CrossRef](#)]
29. Rufai, F.; Folorunso, O.; Lateef, U. Predicting Students' Enrollment Using Generalized Feed-Forward Neural Network. *J. Nat. Sci. Eng. Technol.* **2015**, *14*, 58–70. [[CrossRef](#)]
30. Suman, S.; Singh, V.; Rathod, T.; Wesley, J.C. Runoff Modeling using ANN-based Generalized Feed Forward (GFF) and Multi Linear Regression (MLR) Technique for Narmada River Basin. *Gujarat. Int. J. Curr. Microbiol. Appl. Sci.* **2021**, *10*, 247–257.
31. Spyropoulos, G.C.; Nastos, P.T.; Moustris, K.P. Performance of Aether Low-Cost Sensor Device for Air Pollution Measurements in Urban Environments. Accuracy Evaluation Applying the Air Quality Index (AQI). *Atmosphere* **2021**, *12*, 1246. [[CrossRef](#)]
32. Nastos, P.; Moustris, K.; Larissi, I.; Paliatsos, A. Air Quality and Bioclimatic Conditions within the Greater Athens Area, Greece—Development and Applications of Artificial Neural Networks. In *Advanced Air Pollution 2011*; Nejadkoorki, F., Ed.; InTech-Open Access Publisher: London, UK, 2011; pp. 557–584. ISBN 978-953-307-511-2.
33. Ogliari, E.; Guilizzoni, M.; Giglio, A.; Pretto, S. Wind power 24-h ahead forecast by an artificial neural network and an hybrid model: Comparison of the predictive performance. *Renew. Energy* **2021**, *178*, 1466–1474. [[CrossRef](#)]
34. Qingyu, T.; Shihong, M.; Fuxing, Y.; Weichen, Y.; Yujun, L.; Zhong, Z. An improved wind power uncertainty model for day-ahead robust scheduling considering spatio-temporal correlations of multiple wind farms. *Int. J. Electr.* **2023**, *145*, 108674.
35. Yun, W.; Tuo, C.; Runmin, Z.; Dongran, S.; Fan, Z.; Lingjun, Z. Ensemble probabilistic wind power forecasting with multi-scale features. *Renew. Energy* **2022**, *201 Pt 1*, 734–751.
36. Hellenic Electricity Distribution Network Operator. 2021. Manual—Development Plan of Non-Interconnected Island Systems. Available online: <https://www.rae.gr> (accessed on 17 March 2023).

Disclaimer/Publisher's Note: The statements, opinions and data contained in all publications are solely those of the individual author(s) and contributor(s) and not of MDPI and/or the editor(s). MDPI and/or the editor(s) disclaim responsibility for any injury to people or property resulting from any ideas, methods, instructions or products referred to in the content.